Int. J. Heat Mass Transfer. Vol. 27, No. 8, pp. 1127–1139, 1984
Printed in Great Britain

0017 9310/84 $3.00 + 0.00
Pergamon Press Ltd.

EXPERIMENTAL STUDY OF NATURAL CONVECTION IN AN INCLINED AIR LAYER

HIDEO INABA
Department of Mechanical Engineering, Kitami Institute of Technology, Kitami, Hokkaido 090, Japan

(*Received* 10 *January* 1983 *and in revised form* 27 *July* 1983)

Abstract—The natural convection motion and heat transfer rate in an inclined rectangular air layer, in which two opposing isothermal rigid-boundaries were kept at different temperatures, were investigated experimentally for various angles of inclination, $\theta = 0°$–$180°$, various aspect ratios, $H/W = 5$–83 (height to width of rectangular cavity), and Rayleigh numbers, $Ra_W = 1.2 \times 10^3$–2×10^6. Flow patterns in two planes (X–Y and Y–Z planes) which met at right angles to each other were visualized for various factors mentioned above. Moreover, the non-dimensional correlation equations of the heat transfer rate across the air layer were derived in the relationship between the Nusselt number, Nu_W, and the modified Rayleigh number, $Ra_W \cos\theta$ for $0° \leqslant \theta \leqslant 60°$ or $Ra_W \sin\theta$ for $60° < \theta \leqslant 120°$. The equations proposed agree well with the results of heat transfer measurements from other studies.

NOMENCLATURE

D	depth of rectangular cavity (Z-direction)
g	gravitational acceleration
H	height of rectangular cavity
H/W	aspect ratio
h	local heat transfer coefficient, $q/\Delta T$
h_m	mean heat transfer coefficient, $(1/H)\int_0^H h\,dX$
Nu_X	local Nusselt number, hX/λ
Nu_W	mean Nusselt number, $h_m W/\lambda$
q	local mean flux, $q_{cd} + q_{cv} = q_T - q_{\theta=180°} + q_{cd}$
q_m	mean heat flux, $(1/H)\int_0^H q\,dX$
q_T	total heat flux, $q_{cd} + q_{cv} + q_{ra} + q_l$
q_{cd}	thermal conductive heat flux
q_{cv}	convective heat flux
q_l	heat flux based on the heat loss of the experimental apparatus
q_{ra}	radiant heat flux
$q_{\theta=180°}$	total heat flux at $\theta = 180°$
Ra_W	Rayleigh number, $g\beta\Delta T W^3/\nu\alpha$
T	temperature
ΔT	temperature difference, $T_h - T_c$
W	width of rectangular cavity
X, Y, Z	Cartesian coordinates.

Greek symbols

α	thermal diffusivity
β	thermal expansion coefficient
ε	radiant emissivity
λ	thermal conductivity
ν	kinematic viscosity
θ	inclination angle.

Subscripts

c	cold wall
h	hot wall.

Superscript

*	non-dimensional quantity.

1. INTRODUCTION

THIS study deals with the thermal natural convective motion and heat transfer rate in an inclined narrow rectangular cavity filled with air, whose two opposing isothermal walls are separated by a width, W, and maintained at different temperatures in the wide range of inclination angles, θ, from the horizontal (heated from below). For several years, increasing attention has been paid to the problem of natural convection in inclined fluid layers. The occurrence of an inclined natural convective movement related to the motion of the atmospheric layer and the ocean layer as well as the heat transfer in the building and in cooking vessels is rather common since rarely is the earth's surface aligned with geopotential lines.

Visual observations of flow patterns and heat transfer measurements in the inclined fluid layer have been carried out by a number of researchers up to date. Firstly DeGraaf and Van der Held [1] considered experimentally the inclined convection problem at small inclination angles. Hart [2] performed a series of flow visualization experiments from the top glass plate water jacket for various inclination angles to examine flow instabilities in water. He observed the existence of longitudinal rolls with axes directed up the slope, roll-dominated turbulence and transverse travelling waves depending on inclination angles and temperature differences between the surface temperatures of the hot and cold walls. Ozoe *et al.* [3] reported similar flow behaviors and measurements of the heat transfer rate for aspect ratios $H/W = 1$–15.5 in air as well as higher Prandtl number fluids. Clever and Busse [4] investigated the stability of longitudinal rolls in an inclined convection layer. They reported three types of flow instabilities which were responsible for the transition from longitudinal rolls to three-dimensional

(3-D) flows of convection in different regimes of the parameter space. Ruth *et al.* [5, 6] clarified the convection flow patterns in an inclined air layer ($0° \leqslant \theta \leqslant 30°$ and $10^2 \leqslant Ra_W \cos\theta \leqslant 10^4$). They observed the secondary transition in the convective motion in the regime of $\theta > 20°$. Linthorst *et al.* [7] observed the flow structures of natural convection in inclined air-filled enclosures with the laser Doppler anemometer measurements of velocity profiles in the ranges of $0.25 \leqslant H/W \leqslant 7$, $0° \leqslant \theta \leqslant 90°$ and $5 \times 10^3 \leqslant Ra_W \leqslant 2.5 \times 10^5$. They determined the transition from stationary to non-stationary flow and the transition from 2- to 3-D flow. A review of the heat transfer measurements in inclined enclosures was given by Buchberg *et al.* [8]. That is, the heat transfer rate through the inclined fluid layer was correlated with the non-dimensional relationship between Nu_W and $Ra_W \cos\theta$. Recently, Elsherbiny *et al.* [9] measured the heat transfer rate in the range of aspect ratios $H/W = 5$–110, inclination angles $\theta = 0°$–$90°$ and Rayleigh numbers $Ra_W = 10^2$–2×10^7.

However, in the most recent works mentioned above, visual observations of flow patterns have been performed only from one direction, for example, from the top cooling wall made of a transparent material (glass cover, etc.) in the small range of inclination angles $\theta = 0°$–$90°$. Little attention has been paid to the temperature profile measurements in the fluid layer, which is important for flow and heat transfer behaviors. The primary objective of this paper is to visualize the flow behaviors on two planes (X–Y and Y–Z planes) at right angles to each other in the air-filled inclined rectangular cavity, to obtain the temperature profile of the inclined air layer, and to measure the heat transfer rate through the air layer. The present experiments were carried out under the following conditions:

(a) inclination angles $\theta = 0°$–$180°$;
(b) aspect ratios $H/W = 5$–83;
(c) Rayleigh numbers $Ra_W = 1.2 \times 10^3$–2×10^6.

Moreover, useful non-dimensional correlation equations of the heat transfer rate through the air layer are derived in the wide ranges of inclination angles, aspect ratios and Rayleigh numbers.

2. EXPERIMENTAL APPARATUS AND PROCEDURE

2.1. *Description of experimental apparatus and procedure*

The present experiments were carried out using inclined air-filled rectangular cavities, whose two opposing isothermal walls were kept at different temperatures while the other walls were thermally insulated. The main parts of the experimental apparatus consisted of the heating part, air-filled test section and cooling part as depicted in Fig. 1. Four kinds of test sections were constructed by inserting the bakelite frames (15 mm thick) of 580 mm (fixed height

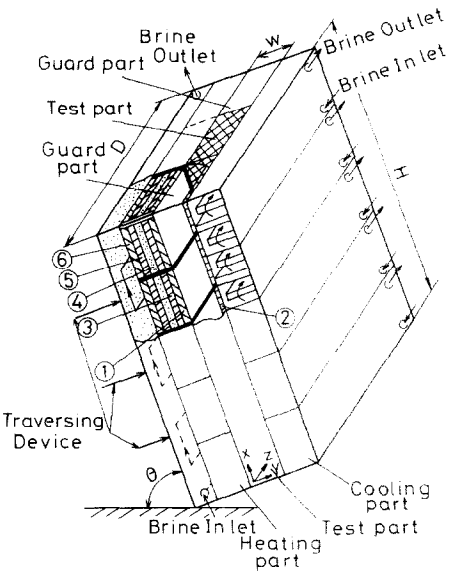

FIG. 1. A schematic diagram of the experimental apparatus: (1) heating wall; (2) cooling wall; (3) main heater; (4) bakelite plate; (5) guard heater; (6) aluminum plate.

H) × 7 mm (aspect ratio $H/W = 83$), 10 mm ($H/W = 58$), 20 mm ($H/W = 29$) and 58 mm ($H/W = 10$) (variable width W) section areas and 400 mm (depth D) between the heating and cooling parts. A center part 200 mm in depth (Z-direction) was used as the test section and both sides (100 mm length) of the test section in the Z-direction were used as the guard parts.

In order to obtain two opposing heating and cooling boundary conditions with a uniform temperature, the hot and cold walls (5 mm thick copper plate) were divided into five parts by 3 mm thick bakelite frames in the X-direction. The surface temperature of the hot wall was maintained at a uniform temperature using five independently controlled main mica electricity heaters (maximum power output of 1 kW). The guard mica heaters were mounted on the rear side of the main heaters across a bakelite plate (5 mm thick) to minimize the heat loss from the main heaters to the environment. Moreover, ten guard mica heaters were equipped in both sides of main heaters in the Z-direction so as to minimize the heat loss from the main heaters.

The surface temperature of the cold wall was maintained at a uniform temperature by introducing temperature-controlled coolant (brine) into each of five separate cooling chambers attached to the rear side of the cold walls. Consequently it was possible to control the surface temperature gradients of the hot and cold walls in the X-direction to within $\pm 2 \times 10^{-3}$ °C cm^{-1}. The temperatures at 50 measuring points (the hot and cold walls, the main and guard heaters) were measured with Cu–Co thermocouples (0.1 mm in diameter). In order to measure the temperature distributions of the air layer, three traversing small probes (0.8 mm diameter stainless steel pipe) with Cu–Co thermocouples (0.1 mm in diameter) which were able to move in the Y-direction were set at positions $X = 145$ mm

($X^* = X/H = 0.25$), 290 mm ($X^* = 0.5$) and 435 mm ($X^* = 0.75$).

In order to minimize the heat loss from the experimental apparatus, the experimental apparatus was covered with styrofoam insulating material to a thickness of 10 cm and was placed into the temperature-controlled room which was at the average of the surface temperatures of the hot and cold walls. The heat loss from the experimental apparatus to the environment was ascertained to be less than $\pm 7\%$ from the results of preliminary experiments, which were carried out by packing liquid paraffin wax of thermal conductivity $\lambda_{cd} = 0.0928\ W\,m^{-1}\,K^{-1}$ at 20°C into the test section at an inclination angle $\theta = 180°$ (heated from above) without natural convection.

The hot and cold walls in the present study consisted of well-polished copper plates with a small radiant emissivity $\varepsilon = 0.06$. The experimental data were taken after the thermal and fluid-dynamic conditions had reached a steady state. It took about 15–20 h to reach the steady state.

The heat flux q_{cv} of the natural convective heat transfer at any inclination angle was determined by subtracting the total heat flux $q_{\theta=180°}$ at $\theta = 180°$ without natural convection from the total heat flux q_T at any inclination angle as follows

$$q_{\theta=180°} = q_{cd} + q_{ra} + q_l, \tag{1}$$

$$q_T = q_{cd} + q_{ra} + q_{cv} + q_l, \tag{2}$$

$$q_{cv} = q_T - q_{\theta=180°}. \tag{3}$$

The physical properties which were used to determine the non-dimensional variables were evaluated at the average of the surface temperatures of the hot and cold walls.

2.2. *Description of visual observation of flow pattern*

Other apparatus, basically similar to the apparatus mentioned above, were constructed in order to study visually the flow behaviors of natural convection. In order to make visual observations of the flow pattern, the test sections were fabricated by inserting transparent frames (10 mm thick lucite frames) of width $W = 22$ mm ($H/W = 5$) between the isothermal hot and cold copper walls (5 mm thick) of fixed height $H = 110$ mm and depth $D = 200$ mm. The hot and cold walls were painted black to prevent reflection of the light beam. To illuminate the X–Y or Y–Z plane of the test section as shown in Fig. 2, a parallel light beam was created by means of an optical setup and a 300 W Hg source. A water filter 20 mm thick was used to minimize the incoming infrared radiation from the light source into the test section. The convection patterns were visualized by introducing cigar smoke through two ports in the test section at a very slow speed. Photographs were taken using a 35 mm camera with close-up and wide angle lenses and 400 ASA film. Typical exposure times at an aperture of 1.4 varied from 2 to 15 s. The experimental apparatus for visualization was placed in the temperature-controlled 'light tight' black room, and covered with styrofoam insulating material (50 mm thick) except during the visualization operating period.

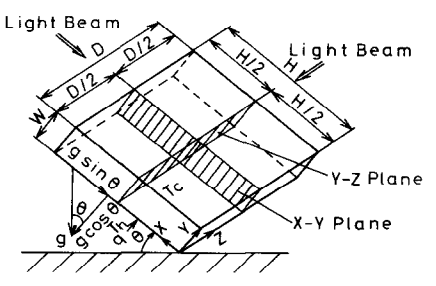

FIG. 2. X–Y plane and Y–Z plane for visual observation (hatched portions).

3. EXPERIMENTAL RESULTS AND DISCUSSIONS

3.1. *Temperature profile of the air layer*

Figures 3(a)–(e) show the typical non-dimensional temperature distributions $T^* = (T - T_c)/(T_h - T_c)$ in the Y^*-direction ($Y^* = Y/W$) for inclination angles $\theta = 0°$, 30°, 90°, 120°, and 150°, respectively, at the fixed positions of $X^* = 0.25$, 0.5, and 0.75 under the conditions of $H/W = 10$ ($W = 58$ mm) and $\Delta T = 100°C$. Typical non-dimensional temperature distributions for the case when $\theta = 0°$ (the heating of a horizontal air layer from below) are presented in Fig. 3(a). It seems that these temperature distributions correspond with those of Bénard convection. That is, the existence of the boundary layer flows, in the horizontal direction, along the hot and cold walls is presumed from the facts of the large temperature gradients in the vicinity of both walls and the small variations of the temperature distribution in the Y^*-direction in the center core region outside of both boundary layer flows. At this inclination angle, $\theta = 0°$, it is intriguing to note that temperature distributions at $X^* = 0.25$, 0.5, and 0.75 make little difference. The behavior of the temperature distributions obtained might be explained from the fact that three probes for air temperature measurement do not traverse in the region of the ascending plume flows of hot air from the hot wall to the cold wall and the descending flows of cold air from the cold wall. Figure 3(b) shows the non-dimensional temperature distributions for $\theta = 30°$. Though the tendency of the temperature distributions for $\theta = 30°$ is basically similar to those for $\theta = 0°$, there appear differences of temperature distributions at three measuring positions ($X^* = 0.25$, 0.5, and 0.75). These differences would mean that the local heat transfer rate on the hot wall becomes large as X^* decreases, since the temperature gradient in the vicinity of the hot wall decreases with an increasing X^*. On the other hand, the local heat transfer rate on the cold wall becomes large as X^* increases since the temperature gradient in the vicinity of the cold wall increases with an increasing X^*. Figure 3(c) presents the non-dimensional temperature distributions for $\theta = 90°$ (the heating of one vertical

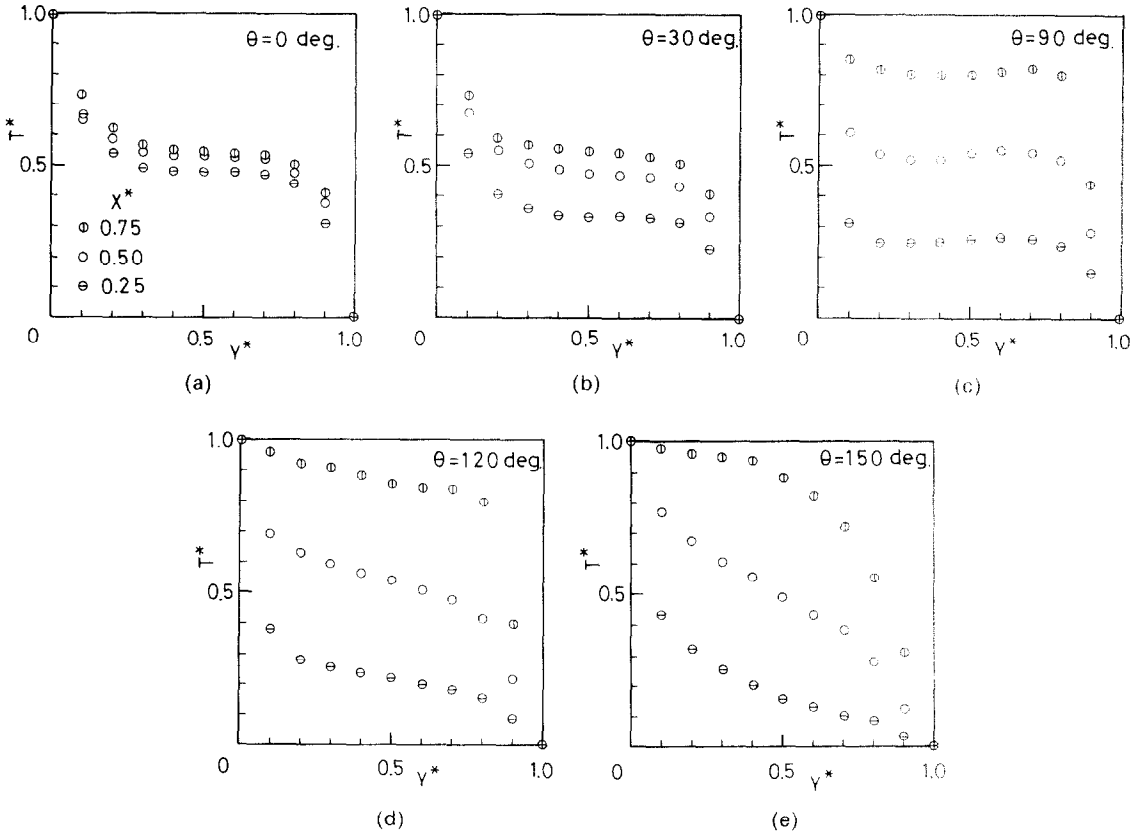

FIG. 3. Non-dimensional temperature profiles for aspect ratio $H/W = 10$ ($W = 58$ mm): (a) $\theta = 0°$; (b) $\theta = 30°$; (c) $\theta = 90°$; (d) $\theta = 120°$; (e) $\theta = 150°$.

wall and the cooling of one opposing vertical wall). These results for $\theta = 90°$ show typical temperature distributions corresponding with a convective flow pattern of the vertical air layer. That is, the decrease and increase of temperature gradients with an increasing X^* appear apparently in the vicinity of the hot wall and the cold wall, respectively. These temperature gradient behaviors indicate the existence of a boundary layer flow which ascends along the hot wall or descends along the cold wall. Moreover, the difference of temperature distributions at three measuring positions for $\theta = 90°$ become large as compared with that for $\theta = 30°$. The temperature distributions for $\theta = 120°$ in which the hot wall exists above and the cold wall exists below are shown in Fig. 3(d). It would be understood that the convective heat transfer rate for $\theta = 120°$ is decreased as compared with that for $\theta = 90°$ since the temperature gradients of both walls are decreased and the variation of temperature in the center core region becomes larger for $\theta = 120°$. Figure 3(e) indicates typical temperature distributions for $\theta = 150°$. It can be seen that the influence of convection becomes small because of the decrease of temperature gradients in the vicinity of the hot and cold walls. Especially, the temperature variation at $X^* = 0.5$ approaches a linear relationship between T^* and Y^*, which means the conductive heat transfer.

3.2. *The flow visualization in an inclined air layer*

Most of the previous studies of flow behaviors were undertaken by viewing the flow field from above in which the upper boundary of the fluid layer was made of a transparent material or by visualizing it only at the X–Y plane as shown in Fig. 2. Little attention has been paid up to date to flow visualization from multi-orientations of flow patterns in different cross-sections. To obtain more detailed information on flow behaviors, the present visual observations were performed by taking photographs of the airflow patterns from two different orientations in different cross-sections, that is, an X–Y plane at $Z = D/2$ and a Y–Z plane at $X = H/2$ as seen in Fig. 2. Cigar smoke as a tracer particle was injected very slowly into the test section from two ports in the test-section frame, and after 2–5 min photographs of the flow patterns were taken in order to overcome the problem of confusing smoke injection effects (the forced convection and diffusion of smoke) with unsteadiness of the natural convection. The visual photographs of comparatively stable flow patterns were obtained in the range $Ra_W = 7 \times 10^3$–6.1×10^4 for $H/W = 5$ ($W = 22$ mm). However, for $Ra_W > 10^5$, it was difficult to obtain clearly visual photographs of the streak-lines of the airflow due to the disturbance of the flow and diffusion of injecting smoke.

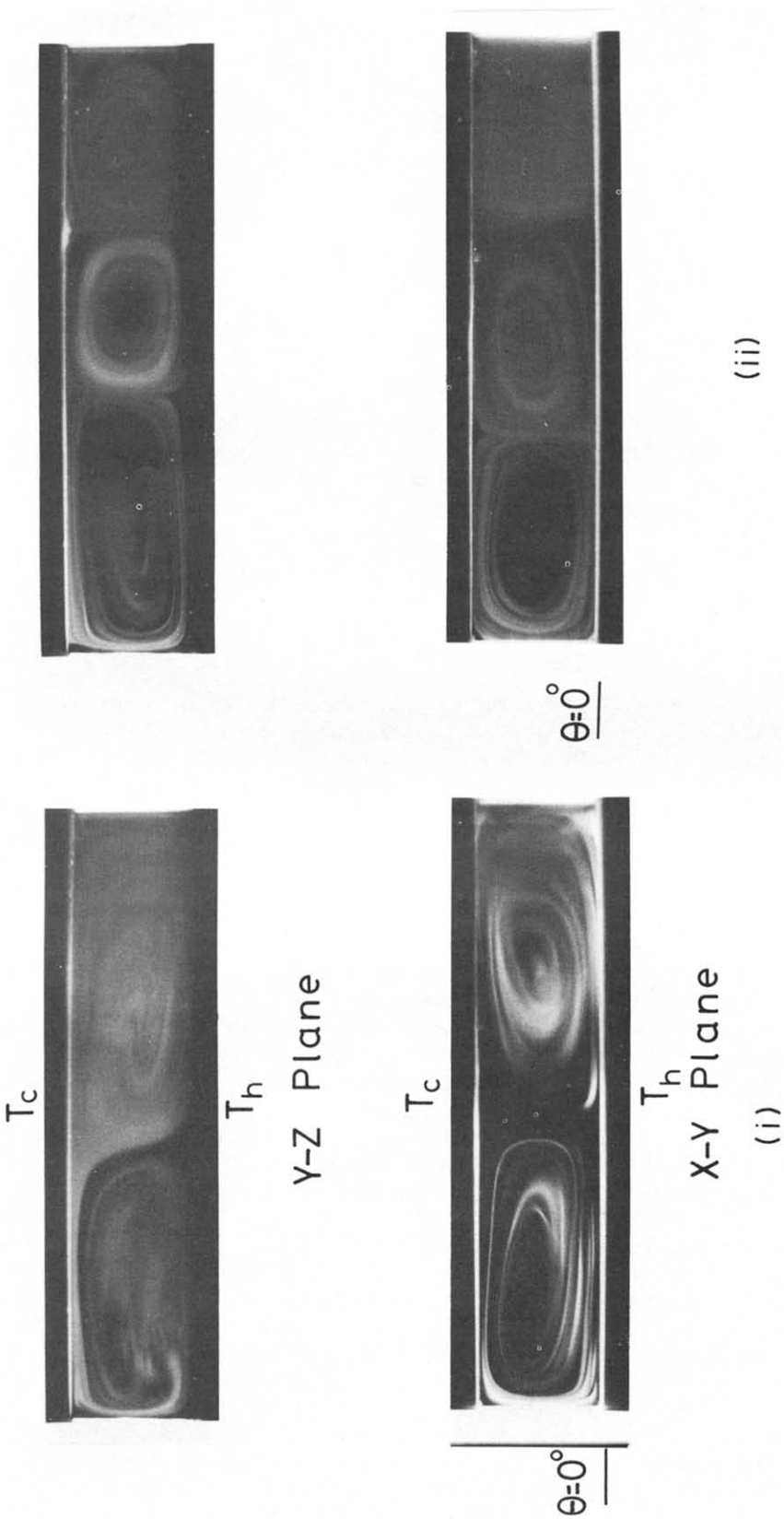

FIG. 4(a). Convective flow patterns at X–Y plane (lower) and Y–Z plane (upper) for $H/W = 5$ ($W = 22$ mm). For $\theta = 0°$: (i) $Ra_W = 7 \times 10^3$; (ii) $Ra_W = 1.9 \times 10^4$.

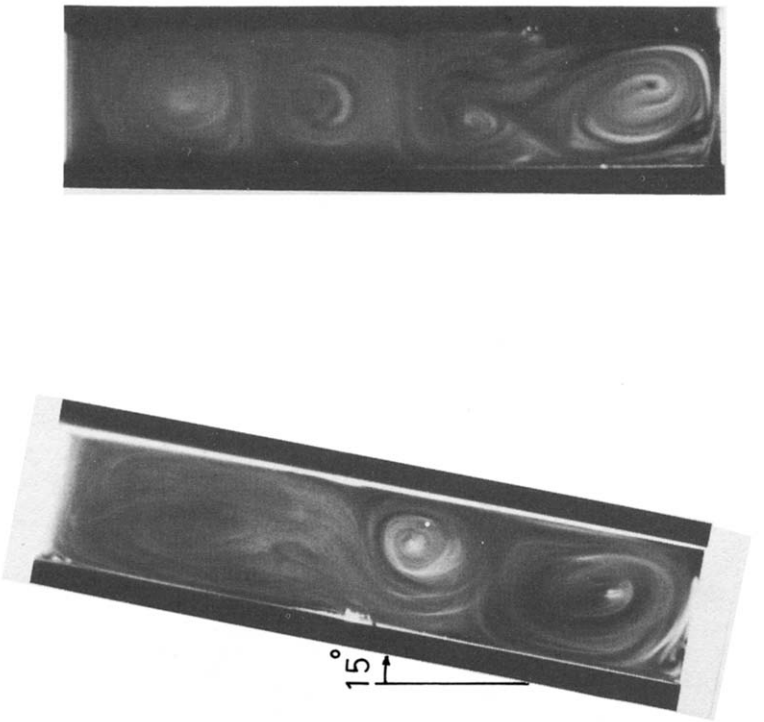

FIG. 4(b). As Fig. 4(a) but for $\theta = 15°$: $Ra_W = 2.6 \times 10^4$.

Typical examples of the change in the flow pattern with various inclination angles $\theta = 0°$–$150°$ and Rayleigh numbers $Ra_W = 7 \times 10^3$–6×10^4 are shown in Figs. 4(a)–(g) for $H/W = 5$. For $\theta = 0°$, at $Ra_W = 7 \times 10^3$ both visual photographs on the X–Y and Y–Z planes in Fig. 4(a) (i) show two stable rolls (Bénard cellular flows) which circulate each other in opposite directions. For the case of $Ra_W = 1.9 \times 10^4$ in Fig. 4(a) (ii), a number of stable convective rolls can be observed and the circulation speed of them becomes faster.

For $\theta = 15°$, at $Ra_W = 2.6 \times 10^4$ streak-lines of the flow are presented in Fig. 4(b). On the X–Y plane, a stable cellular flow appears at the lower part of the inclined cavity and an unstable flow pattern is observed at the upper part. While on the Y–Z plane, four unstable rolls are recognized.

For $\theta = 30°$, Fig. 4(c) (i) shows photographs of the flow patterns at $Ra_W = 1.9 \times 10^4$. The flow behavior on the X–Y plane in this photograph is similar to that for $\theta = 15°$ as shown in Fig. 4(b). At $Ra_W = 5.1 \times 10^4$ in Fig. 4(c) (ii), an instability of the flow is increased as compared with results at $Ra_W = 1.9 \times 10^4$.

For $\theta = 60°$, the flow behaviors at $Ra_W = 2.1 \times 10^4$ are presented in Fig. 4(d). A comparatively stable unicellular flow is observed on the X–Y plane, on the other hand, complex multi-cellular rolls are recognized on the Y–Z plane. These flow behaviors might correspond to the convoluted flow (spiral or coil flow) climbing up along the slope direction.

For $\theta = 90°$, Fig. 4(e) shows photographs of the streak-lines of the airflow at $Ra_W = 6.1 \times 10^4$. On the X–Y plane, the boundary layer flows, that is, an ascending flow along the hot wall and a descending flow along the cold wall appear in the vertical air layer, and these flows are very stable. While it would be recognized that there exist very stably complicated flows on the Y–Z plane.

For $\theta = 120°$, the flow patterns at $Ra_W = 2 \times 10^4$ are shown in Fig. 4(f). These flow behaviors are similar to those for $\theta = 90°$ but flow speed for $\theta = 120°$ becomes slower than it is for $\theta = 90°$.

For $\theta = 150°$, the flow behaviors at $Ra_W = 1.9 \times 10^4$ in Fig. 4(g) are similar to those for $\theta = 120°$, however, these flow speeds become closer in comparison with those for $\theta = 120°$.

From the results of flow visualizations for $H/W = 5$, it could be understood that multi-cellular flows (Bénard convection) exist in the range of inclination angles below 15°, convoluted rolls (spiral flows) with axes oriented up to the slope are recognized in the range of $\theta = 30°$–$60°$ and unicellular boundary layer flow appears in the range of $\theta = 90°$–$150°$ for $Ra_W = 7 \times 10^4$–6.1×10^4.

3.3. *Local heat transfer in the X*-direction on the hot wall*

Figure 5 for $H/W = 10$ ($W = 58$ mm) presents typical profiles for the local Nusselt number Nu_X in the X^*-direction on the hot wall. ($Y^* = 0$), which were obtained by measuring each heat input at five independent heating surfaces as mentioned in terms of the description of the experimental apparatus. In Fig. 5, it is shown that the change of local Nusselt number Nu_X is independent of the distance X^* for an inclination angle $\theta = 0°$, the values of Nu_X for $\theta = 15°$ and 30° decrease gradually with increasing X^*. This independency or small dependency of the local Nusselt

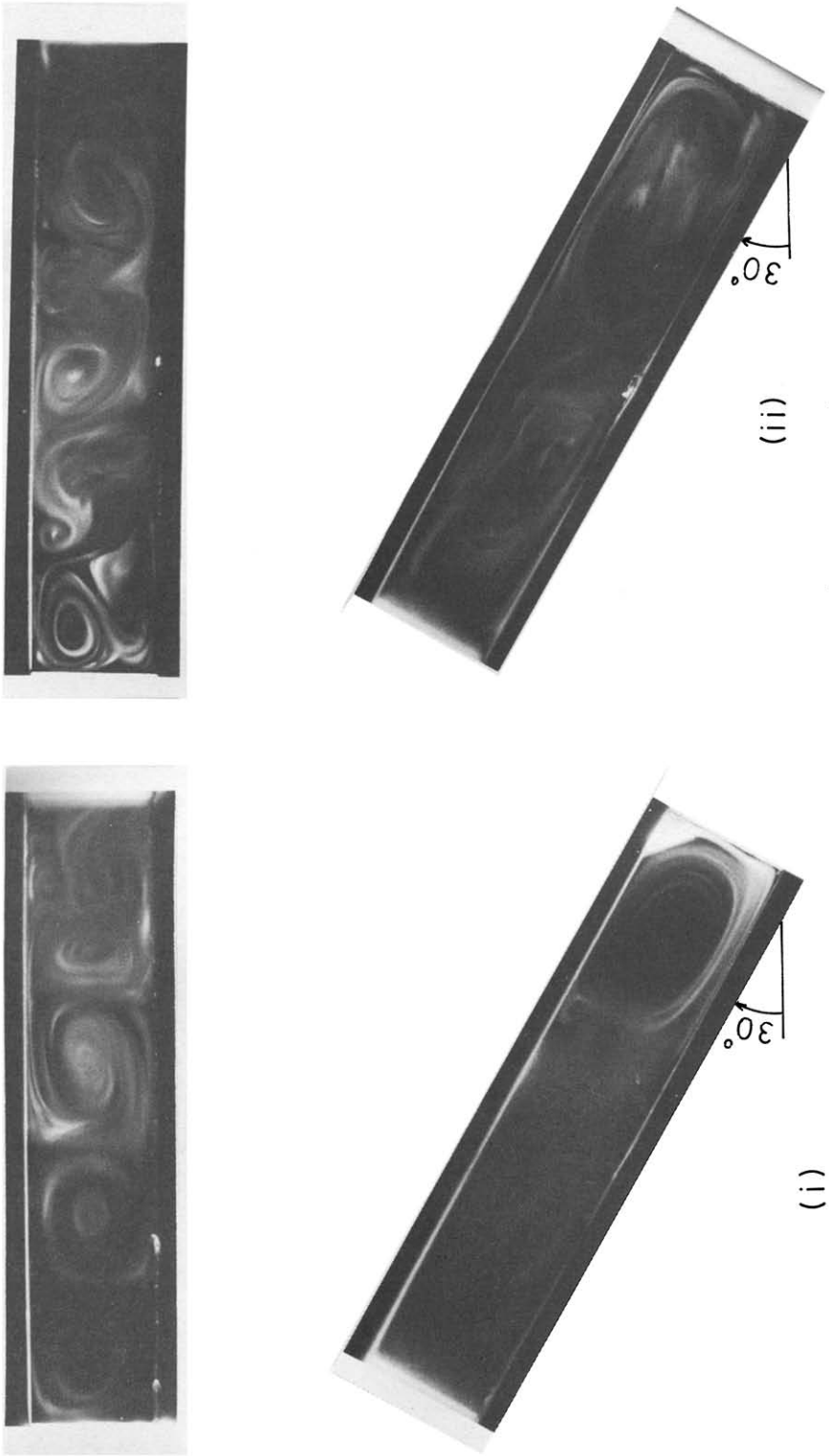

FIG. 4(c). As Fig. 4(a) but for $\theta = 30°$: (i) $Ra_W = 1.9 \times 10^4$; (ii) $Ra_W = 5.1 \times 10^4$.

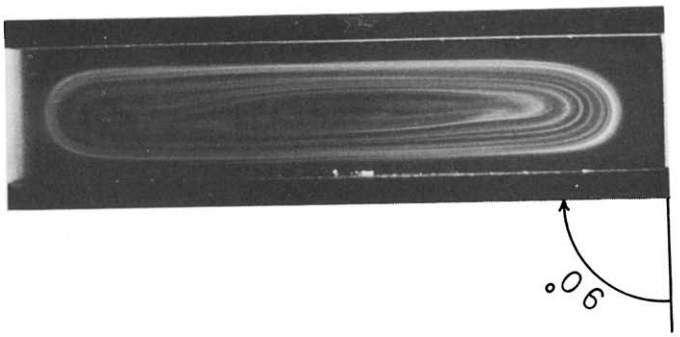

FIG. 4(c). As Fig. 4(a) but for $\theta = 90°$; $Ra_{\delta T} = 6.1 \times 10^4$.

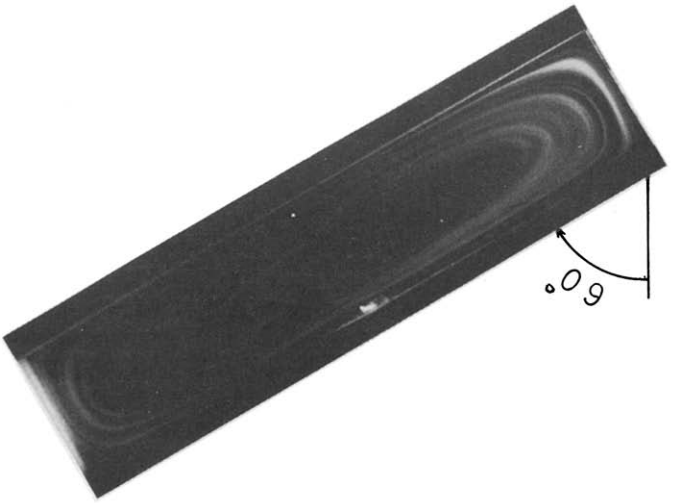

FIG. 4(d). As Fig. 4(a) but for $\theta = 60°$; $Ra_{\delta T} = 2.1 \times 10^4$.

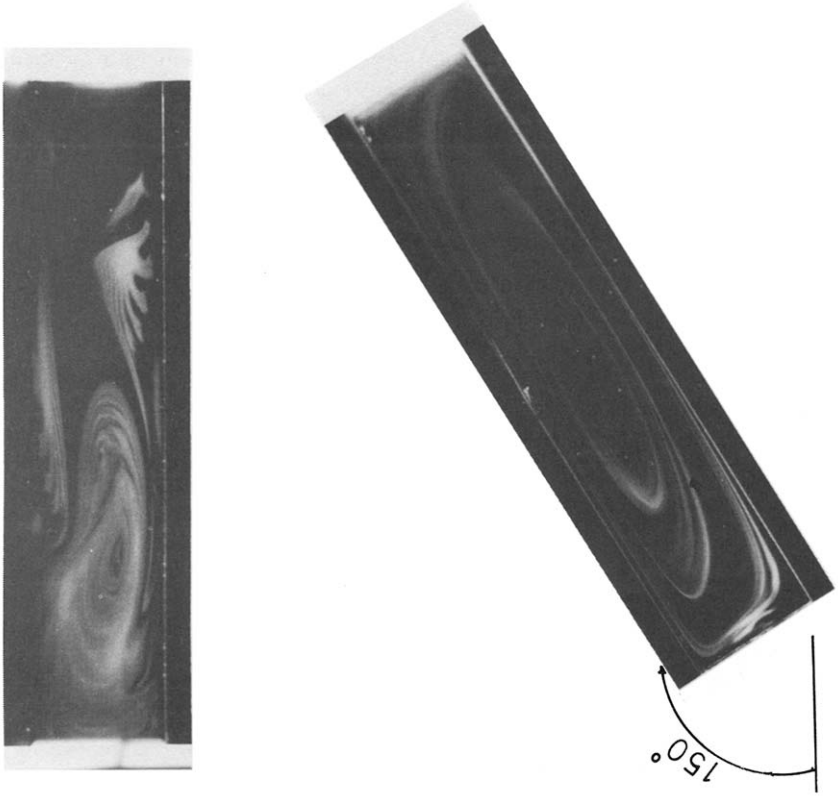

FIG. 4(g). As Fig. 4(a) but for $\theta = 150°$: $Ra_w = 1.9 \times 10^4$.

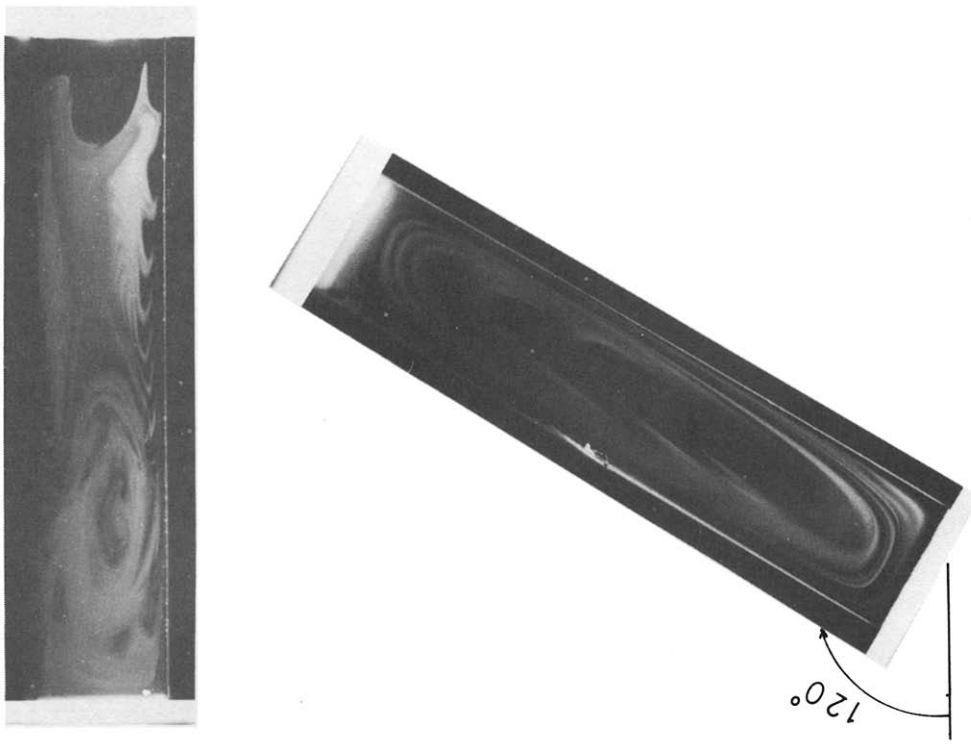

FIG. 4(f). As Fig. 4(a) but for $\theta = 120°$: $Ra_w = 2.0 \times 10^4$.

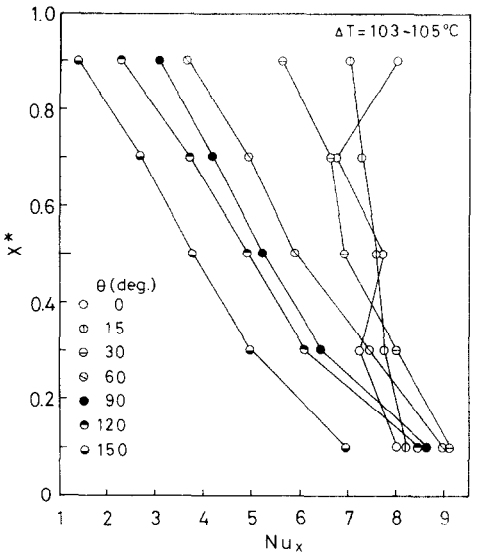

FIG. 5. Local Nusselt number Nu_X distributions in the X^*-direction on the hot wall for $H/W = 10$ ($W = 58$ mm).

number's distribution to the distance X^* could be explained that in the small inclination angle ($0° \leqslant \theta \leqslant 30°$), the heat transfer from the hot wall to the cold wall was carried out mainly by multi-cellular flows as could be seen in visual observations mentioned above, which reduce the distribution of local heat transfer rate on the hot wall since the hot air from the hot wall arrived at the cold wall through many short-cut paths in the air layer due to the existence of multi-cellular flows. In case of $\theta = 60°$, the local Nusselt number Nu_X is decreased gradually with increasing X^*. This tendency of Nu_X to X^* may be induced by the convoluted flow (spiral flow) as could be shown in Fig. 4(d). For $\theta = 90°$ and 120°, it might be understood that the decreasing rate of Nu_X to X^* becomes large in small X^*. This behavior of the local Nusselt number's change could be explained by the fact that the value of Nu_X in small X^* becomes large and it decreases gradually with increasing X^* because of a collision of cold air from the cold wall with the hot wall in the range of small X^* and a development of boundary layer flow along the hot wall as seen in Figs. 4(e) and (f). The variation of Nu_X to X^* for $\theta = 150°$ is similar to it for $\theta = 90°$–120°, however, the value of Nu_X becomes smaller than that for $\theta = 90°$ or 120°.

3.4. *Effect of inclination angle θ on the average Nusselt number Nu_W*

Figure 6 presents the relationship between the inclination angle θ and the average Nusselt number Nu_W for various aspect ratios H/W under the temperature difference $\Delta T = 103$–105°C. In this figure, for small aspect ratios $H/W = 10$ and 29, the value of Nu increases slightly on increasing the inclination angle from $\theta = 0°$ to about 15°, it has a maximum value of Nu_W at about 15°. The value of Nu_W with increasing θ decreases steeply from $\theta = 30°$ to 60°, next the decreasing rate of Nu_W becomes small in the range of $\theta = 60°$–120°, and finally in the range of $\theta > 120°$ the value of Nu_W decreases steeply again. These complex behaviors of Nu_W to θ could be explained as follows:

For $0° \leqslant \theta < 30°$, the development of multi-cellular flows (Bénard convection) with inclination angle θ would induce the slight increase of Nu_W as could be seen in the flow patterns in Figs. 4(a) and (b). For $30° \leqslant \theta \leqslant 60°$, the existence of convoluted flows (spiral flow) with their axes oriented up the slope causes the steep decrease of Nu_W with increasing θ since the short-cut flows through the air layer become less as the inclination angle increases. For $60° < \theta \leqslant 120°$, the boundary layer flow (a unicellular flow) developing in the vicinity of the hot wall or cold wall would bring the small decrease of Nu_W to θ. For $\theta > 120°$, the decreasing rate of Nu_W with θ becomes large since the contribution of the convection to the heat transfer is reduced steeply by increasing the degree of the heating from above.

From this figure, it would be also understood that the decreasing rate of Nu_W with θ becomes small for large aspect ratios $H/W = 58$ and 83. For $H/W = 58$, the value of Nu_W becomes unity in which the contribution of the convection to the heat transfer is negligible at about $\theta = 75°$, while it becomes unity at about 15° for $H/W = 83$.

3.5. *Non-dimensional correlation equations of heat transfer through the air layer*

In many of the past studies, the relationship between Nu_W and $Ra_W \cos\theta$ has been used to non-dimensionalize the data of the heat transfer in inclined enclosures. However, this non-dimensional correlation is useful only in small inclination angle θ since the value of $\cos\theta$ decreases steeply as the value of θ approached

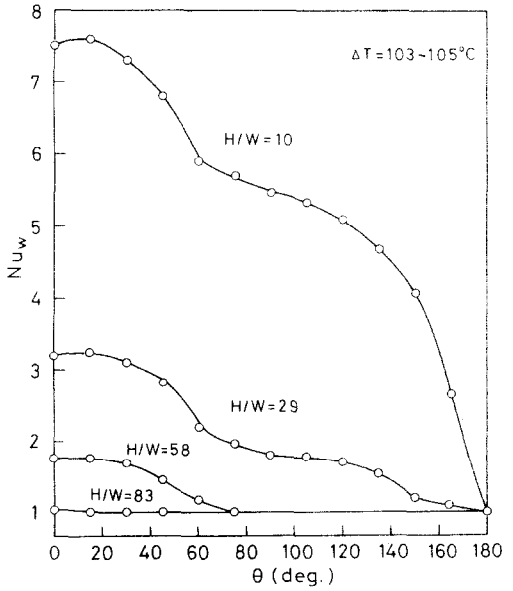

FIG. 6. Relationship between average Nusselt number Nu_W and inclination angle θ for various aspect ratios H/W.

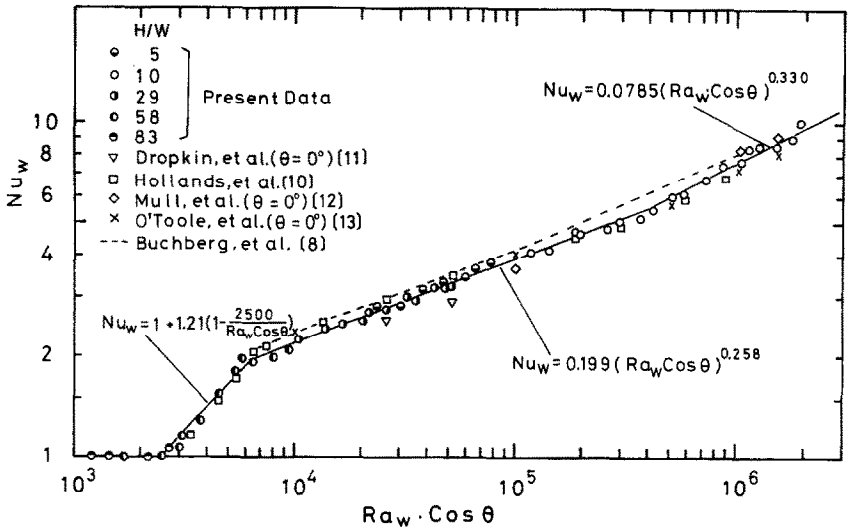

FIG. 7. Relationship between Nu_W and $Ra_W \cos\theta$ for $0° \leqslant \theta \leqslant 60°$.

to 90° ($\cos\theta = 0$ at $\theta = 90°$). Therefore, the present study tried to derive new correlation equations of the heat transfer in the range of large inclination angles. At an inclination angle θ below 60° in which multi-cellular flows or convoluted flows predominate in the air layer as mentioned above, the previous and present data are plotted with the relationship between Nu_W and $Ra_W \cos\theta$ in Fig. 7. From these results of heat transfer in Fig. 7, it could be understood that three non-dimensional correlation equations of the heat transfer are derived according to the range of $Nu_W \cos\theta$ with some accuracy for the sake of simplicity as follows:

(a) Post-conductive region ($2.5 \times 10^3 \leqslant Ra_W \cos\theta \leqslant 6.0 \times 10^3$)

$$Nu_W = 1 + 1.21\left(1 - \frac{2500}{Ra_W \cos\theta}\right). \quad (4)$$

The present equation (4) fits well data reported by Hollands [10].

(b) Laminar flow region ($6 \times 10^3 < Ra_W \cos\theta \leqslant 4 \times 10^5$)

$$Nu_W = 0.199(Ra_W \cos\theta)^{0.258}. \quad (5)$$

Dropkin's [11] and Mull's [12] data for $\theta = 0°$ are a little below the present data and correlation equation (5).

(c) Turbulent flow region ($4 \times 10^5 < Ra_W \cos\theta$)

$$Nu_W = 0.0785(Ra_W \cos\theta)^{0.330}. \quad (6)$$

In this figure, the flow in the air layer becomes turbulent and the increasing rate of Nu_W to $Ra_W \cos\theta$ becomes larger in comparison with the results of laminar flow region in equation (5). The data agree with equations (4)–(6) within a maximum deviation of 7.5%, and

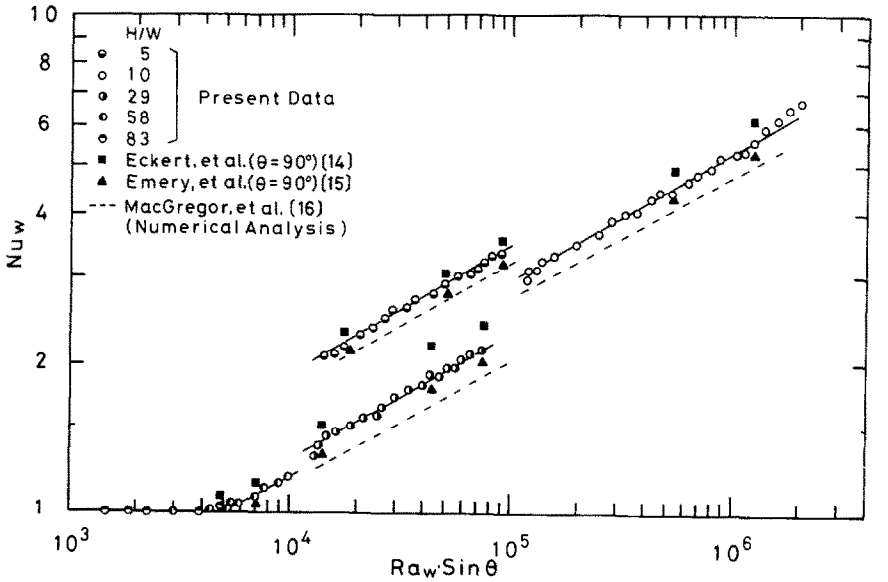

FIG. 8. Relationship between Nu_W and $Ra_W \sin\theta$ for $60° < \theta \leqslant 120°$.

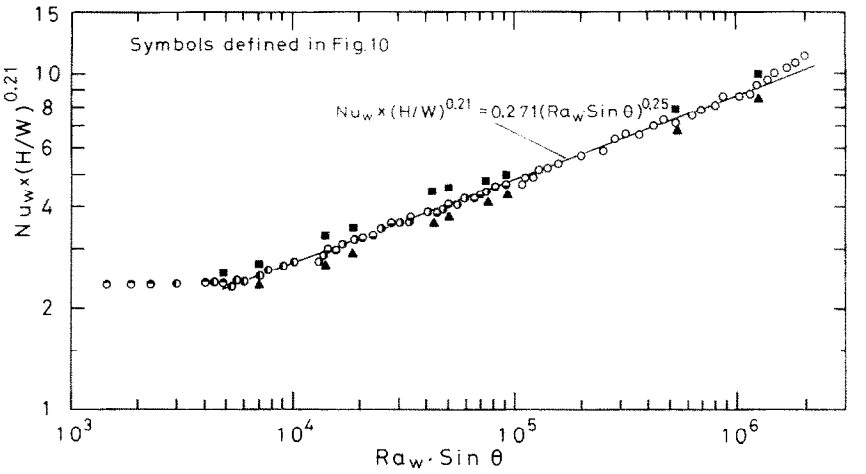

FIG. 9. Relationship between $Nu_W(H/W)^{0.21}$ and $Ra_W \sin\theta$ for $60^\circ < \theta \leqslant 120^\circ$.

these equations can be applicable in the range of $0^\circ \leqslant \theta \leqslant 60^\circ$.

At an inclination angle θ above 60°, the previous and present data are plotted with the relationship between Nu_W and $Ra_W \sin\theta$ as seen in Fig. 8. In this figure, it could be understood that the value of Nu_W depends on not only the $Ra_W \sin\theta$ but also aspect ratio H/W. From these results, the following non-dimensional correlation equation can be derived with some accuracy for the sake of simplicity

$$Nu_W = 0.271(H/W)^{-0.21}(Ra_W \sin\theta)^{0.250}, \quad (7)$$

for laminar flow region ($5 \times 10^3 \leqslant Ra_W \sin\theta \leqslant 1.2 \times 10^6$ and $5 \leqslant H/W \leqslant 83$). Figure 9 shows the relationship between $Nu_W(H/W)^{0.21}$ and $Ra_W \sin\theta$ from the result of equation (7). The data agree well with equation (7) within a maximum deviation of 6%. At the $Ra_W \sin\theta$ above 1.2×10^6, the data are plotted over the correlation curve of equation (7). The increase of Nu_W to $Ra_W \sin\theta$ would mean the occurrence of the turbulent flow.

4. CONCLUSIONS

Flow and heat transfer behaviors in an inclined air layer have been clarified experimentally by the flow visualizations and the measurements of temperature profiles and heat transfer through the air layer in the wide ranges of inclination angles $\theta = 0^\circ \sim 150^\circ$, aspect ratios $H/W = 5 \sim 83$ and the Rayleigh numbers $Ra_W = 1.2 \times 10^3 \sim 2 \times 10^6$.

(1) Three types of flow patterns in the laminar flow region are recognized according to the inclination angle θ. For $\theta = 0^\circ \sim 30^\circ$, there exist mainly multicellular flows (Bénard convection). For $\theta = 30^\circ \sim 60^\circ$, the convoluted flows (spiral flows) with their axes directed to up slope are recognized in the inclined air layer. For $\theta = 60^\circ \sim 150^\circ$, a unicellular flow (boundary layer flow) exists in the inclined air layer.

(2) For small aspect ratios $H/W = 10 \sim 29$, it is clear that the change of Nusselt number Nu_W to an inclination angle θ becomes complex because of the difference of flow patterns mentioned above, that is, the value of Nu_W has a maximum value at about 15°, it decreases steeply with increasing θ for $\theta = 15^\circ$–60°, the decreasing rate of Nu_W to θ becomes small in the range of $\theta = 60^\circ$–120°, and the value of Nu_W decreases steeply again for $\theta > 120^\circ$.

(3) The data of heat transfer are non-dimensionalized with the relationship between Nu_W and $Ra_W \cos\theta$ for $0^\circ \leqslant \theta \leqslant 60^\circ$. On the other hand, for $60^\circ < \theta \leqslant 120^\circ$ they are non-dimensionalized with the relationship between Nu_W and $Ra_W \sin\theta$. Four kinds of non-dimensional experimental correlation equations of heat transfer rate are derived according to the range of $Ra_W \cos\theta$ or $Ra_W \sin\theta$.

Acknowledgement—The author would like to acknowledge the very capable technical assistance of Mr Fukuda in conducting the present experiments.

REFERENCES

1. G. Z. DeGraaf and E. F. M. Van der Held, The relation between the heat transfer and the convection phenomena in enclosed plane air layers, *Appl. Scient. Res.* **A3**, 393–409 (1953).
2. J. E. Hart, Stability of the flow in a differentially heated inclined box, *J. Fluid Mech.* **47**, 547–576 (1971).
3. H. Ozoe, H. Sayama and S. Churchill, Natural convection in an inclined rectangular box heated from below, *Int. J. Heat Mass Transfer* **20**, 123–129 (1977).
4. R. M. Clever and F. H. Busse, Instabilities of longitudinal convection rolls in an inclined layer, *J. Fluid Mech.* **81**, 107–127 (1977).
5. D. W. Ruth, K. G. T. Hollands and G. D. Raithby, On free convection experiments in inclined air layers heated from below, *J. Fluid Mech.* **96**, 461–479 (1980).
6. D. W. Ruth, G. D. Raithby and K. G. T. Hollands, On the secondary instability in inclined layers, *J. Fluid Mech.* **96**, 481–492 (1980).
7. S. J. M. Linthorst, Wm. M. Schinkel and C. J. Hoogendoorn, Flow structure with natural convection in inclined air-filled enclosures, *Trans. Am. Soc. Mech. Engrs.* Series C, *J. Heat Transfer* **103**, 535–537 (1981).
8. H. Buchberg, I. Catton and D. K. Edward, Natural

convection in enclosed space—a review of application to solar energy collection, *Trans. Am. Soc. Mech. Engrs*, Series C, *J. Heat Transfer* **98,** 182–188 (1976).
9. S. M. Elsherbiny, G. D. Raithby and K. G. T. Hollands, Heat transfer by natural convection across vertical and inclined air layers, *Trans. Am. Soc. Mech. Engrs*, Series C, *J. Heat Transfer* **104,** 96–102 (1982).
10. K. T. G. Hollands and L. Konicek, Experimental study of the stability of differentially heated inclined air layers, *Int. J. Heat Mass Transfer* **16,** 1467–1476 (1973).
11. D. Dropkin and E. Somerscales, Heat transfer by natural convection in liquids confined by two parallel plates which are inclined at various angles with respect to the horizontal, *Trans. Am. Soc. Mech. Engrs*, Series C, *J. Heat Transfer* **87,** 77–84 (1965).
12. W. Mull and H. Reiher, Der Wärmeshutz von luftshichten, Gesundh-Ing. Reihe 1, no. 28 (1930).
13. J. L. O'Toole and P. L. Silveston, Correlations of convective heat transfer in confined horizontal layers, *Chem. Engng Prog. Symp. Ser.* **57,** 81–89 (1961).
14. E. R. G. Eckert and W. O. Carlson, Natural convection in an air layer enclosed between two vertical plates with different temperatures, *Int. J. Heat Mass Transfer* **2,** 106–120 (1961).
15. A. F. Emery and N. C. Chu, Heat transfer across vertical layers, *Trans. Am. Soc. Mech. Engrs*, Series C, *J. Heat Transfer* **87,** 110–116 (1965).
16. R. K. MacGregor and A. F. Emery, Free convection through vertical plane layers, *Trans. Am. Soc. Mech. Engrs*, Series C, *J. Heat Transfer* **91,** 391–402 (1969).

ETUDE EXPERIMENTALE DE LA CONVECTION NATURELLE DANS UNE COUCHE D'AIR INCLINEE

Résumé—On étudie expérimentalement le mouvement de convection naturelle et le transfert thermique dans une couche d'air rectangulaire et inclinée, avec deux frontières rigides, opposées, isothermes à des températures différentes, pour des angles d'inclinaison entre 0° et 180°, plusieurs rapports de forme H/W (hauteur sur largeur de la cavité) entre 5 et 83 et des nombres de Rayleigh $Ra_W = 1{,}2 \times 10^3$–2×10^6. Des configurations d'écoulements dans deux plans (plans XY et YZ) qui se recontrent à angle droit, sont visualisées pour différents facteurs mentionnés ci-dessus. Des formules adimensionnelles donnant le flux thermique transféré à travers la couche d'air sont proposées qui expriment le nombre de Nusselt Nu_W et le nombre de Rayleigh modifié $Ra_W \cos\theta$, pour $0° \leqslant \theta \leqslant 60°$ ou $Ra_W \sin\theta$ pour $60° < \theta \leqslant 120°$. Ces relations s'accordent bien avec les résultats des mesures thermiques d'autres auteurs.

EXPERIMENTELLE UNTERSUCHUNG DER NATÜRLICHEN KONVEKTION IN EINER GENEIGTEN LUFTSCHICHT

Zusammenfassung—Strömung und Wärmeübertragung bei natürlicher Konvektion in einer geneigten rechteckigen Luftschicht mit zwei gegenüberliegenden, starren isothermen Begrenzungen unterschiedlicher Temperatur wurden experimentell untersucht. Dabei wurden variiert: Neigungswinkel $\theta = 0°$–$180°$, Seitenverhältnis $H/W = 5$–83 (Höhe zu Dicke des Rechteckspaltes) und Rayleigh-Zahl $Ra_W = 1{,}2 \times 10^3$–2×10^6. Für viele der angeführten Parameter wurde der Strömungsverlauf in zwei zueinander rechtwinkligen Eben (X–Y und Y–Z Ebene) sichtbar gemacht. Weiter wurden für den Wärmetransport durch die Luftschicht dimensionslose Korrelationen zwischen der Nusselt-Zahl Nu_W und der modifizierten Rayleigh-Zahl $Ra_W \cos\theta$ für $0° \leqslant \theta \leqslant 60°$ oder $Ra_W \sin\theta$ für $60° < 0 \leqslant 120°$ hergeleitet. Die vorgeschlagenen Korrelationen zeigen gute Übereinstimmung mit Wärmeübergangsmessungen anderer Untersuchungen.

ЭКСПЕРИМЕНТАЛЬНОЕ ИССЛЕДОВАНИЕ ЕСТЕСТВЕННОЙ КОНВЕКЦИИ В НАКЛОННОМ СЛОЕ ВОЗДУХА

Аннотация—Проведено экспериментальное исследование естественной конвекции и коэффициента теплопереноса в расположенном под различными углами ($\theta = 0°$–$180°$) прямоугольном слое воздуха, две противоположные жесткие границы которого поддерживаются при различных температурах. Исследовались слои с различными значениями отношения сторон H/W (высота к ширине), изменяющимися в диапазоне от 5 до 83 в интервалах чисел Рэлея $Ra_W = 1{,}2 \times 10^3$–2×10^6. Картины течения в двух перпендикулярно расположенных плоскостях X–Y и Y–Z визуализировались при различных указанных выше значениях параметров. Кроме того, для нахождения коэффициента теплопереноса поперек слоя воздуха выведены соотношения между числом Нуссельта Nu_W и модифицированным числом Рэлея $Ra_W \cos\theta$ для $0° \leqq \theta \leqq 60°$ или $Ra_W \sin\theta$ для $60° < \theta \leqq 120°$. Предложенные соотношения хорошо согласуются с результатами измерений теплопереноса в других работах.